Energy enhancement in time-reversed ultrasonically encoded optical focusing using a photorefractive polymer

Yuta Suzuki
Xiao Xu
Puxiang Lai
Lihong V. Wang

Energy enhancement in time-reversed ultrasonically encoded optical focusing using a photorefractive polymer

Yuta Suzuki, Xiao Xu, Puxiang Lai, and Lihong V. Wang
Washington University in St. Louis, Optical Imaging Laboratory,
Department of Biomedical Engineering, St. Louis, Missouri 63130

Abstract. Time-reversed ultrasonically encoded (TRUE) optical focusing achieves light focusing into scattering media beyond one transport mean free path, which is desirable in biomedical optics. However, the focused optical energy needs to be increased for broad applications. Here, we report the use of a photorefractive polymer (PRP) as the phase conjugate mirror in TRUE optical focusing. The PRP boosted the focused optical energy by ~40 times in comparison to the previously used photorefractive $Bi_{12}SiO_{20}$ crystal. As a result, we successfully imaged absorbing objects embedded in the middle plane of a tissue-mimicking phantom having an optical thickness of 120 scattering mean free paths. © 2012 Society of Photo-Optical Instrumentation Engineers (SPIE). [DOI: 10.1117/1.JBO.17.8.080507]

Dynamic focusing of light into thick biological tissue is desired for noninvasive optical imaging, diagnostics, manipulation, and therapy. However, multiple light scattering in biological tissue limits the focusing of ballistic photons to shallow depths of about one transport mean free path. To solve this problem, Xu et al. developed a technique named time-reversed ultrasonically encoded (TRUE) optical focusing.[1] Using a focused ultrasound (US) beam, the technique spectrally tags the diffuse coherent light inside a scattering medium. Optical focusing into the medium is achieved by selectively phase conjugating, or time-reversing, only the tagged light, using a photorefractive (PR) crystal as a phase conjugate mirror (PCM). Recently, Lai et al. implemented a TRUE optical focusing system in reflection mode,[2] which demonstrated a round-trip optical penetration of 80 scattering mean free paths.

These systems used a photorefractive $Bi_{12}SiO_{20}$ (BSO) crystal as a PCM. However, the transverse dimension of the BSO crystal, like all other inorganic PR crystals, is at most a few centimeters,[3] which limits the area for diffuse light collection.

Address all correspondence to: Lihong V. Wang, Washington University in St. Louis, Optical Imaging Laboratory, Department of Biomedical Engineering, St. Louis, Missouri 63130. Tel: 314-935-6152; Fax: 314-935-7448; E-mail: lhwang@wustl.edu

Furthermore, BSO has other inferior figures of merit, such as its hologram persistency, its PR response time, and its holographic diffraction efficiency. Photorefractive polymers (PRP) show exciting potential to overcome these limitations. Recent studies have demonstrated PRPs with large active areas and high diffraction efficiencies[3] (close to 100%). Further, PRPs can be tuned to have long hologram persistency,[4] or fast response time (~ms).[5] Thus, PRPs can improve TRUE optical focusing by increasing focused energy or accelerating focusing. In this letter, we report the first study using a PRP as the PCM in TRUE optical focusing to enhance focused energy.

The PRP, supplied by Nitto Denko Technical, has the same polymer composite as the one reported in Ref. 4, and consists of a 100-μm-thick polymer film sandwiched between two indium-tin-oxide (ITO) coated glass electrodes. The working wavelength of our polymer is set around our laser wavelength (532 nm). The inset of Fig. 1(a) compares the dimensions of the PRP and BSO crystal used in the previous and current experiments. While the BSO crystal has an active area of 1×1 cm^2, the PRP has an active area of 5×5 cm^2, yielding an etendue ~25 times as large with the same collection geometry.

Figure 1(a) shows the TRUE optical focusing experimental setup, which is similar to that of Ref. 1. In this study, the diameter of the sample beam S incident on the scattering sample was 3 mm, and the diameters of both the reference beam R and readout beam R^* were expanded to 30 mm. The PCM was either a BSO crystal or a PRP. When a BSO crystal was used, it was positioned so that its optical surface normal almost bisected the angle (~20- deg) between the incident reference beam R and the diffused sample beam S (hereafter called "scattered S"). To enhance the phase conjugation efficiency,[6] a 2.1-kHz square-waveform voltage with a peak-to-peak amplitude of 8 kV was applied across the optical surface, yielding an electric field of 8 kV/cm. When a PRP was used as the PCM, its surface normal n was horizontally tilted from the propagation direction of the reference beam R by $\theta \sim 30$- deg, as shown in Fig. 1(b). A 4 kV DC voltage was applied between the polymer's front and back surfaces (the corresponding electric field was 400 kV/cm) to enable its PR performance. In the tested tilted geometry, the etendue of the PRP is estimated to be >400 mm^2 sr using its acceptance angle from Ref. 7.

A hologram was recorded then reconstructed in the PR material. In the holographic recording phase, S was switched on, and after diffusively propagating through the sample, was collected to illuminate the PR material. A focused continuous-wave US beam, with a focal pressure of 1 MPa, focal width of ~1 mm, and focal zone length of ~7 mm, was emitted from a 2 MHz transducer (Sonic Concepts, H106), modulating the diffuse light in the sample. The frequency of S was set to 2 MHz above that of R. Therefore, only the ultrasonically down-modulated light S from the sample formed a stationary interference pattern with R, which was recorded in the PR material as a volume hologram. Once S was switched off after 800 ms holographic recording, shutters S1 and S2 were opened to start the readout phase. Then a 50-ms-long R^* pulse—a counter-propagating phase-conjugated version of R—was switched on to read the hologram, which generated S^*, a time-reversed (TR) copy of the tagged light, to achieve optical focusing. After transmitting through the sample a second time, S^* was detected by a silicon
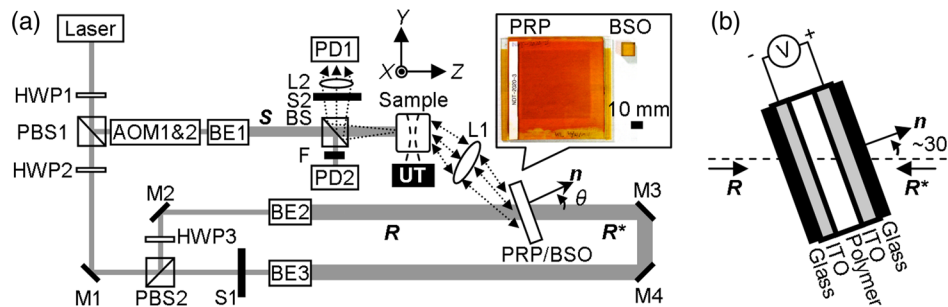
Fig. 1 (a) Schematic of the optical setup used in this study. The inset compares the dimensions of the PRP and BSO crystal. HWP*i*, *i*th halfwave plate; PBS*i*, *i* th polarizing beamsplitter; M*i*, *i* th mirror; AOM*i*, *i*th acousto-optic modulator; BS, beamsplitter; S*i*, *i*th shutter; BE*i*, *i*th beam expander; UT, ultrasound transducer; L*i*, *i*th lens; *F*, neutral density filter. (b) Schematic of high-voltage application to PRP.

photodiode (PD1) as the TRUE signal. Under these experimental conditions, the holographic diffraction efficiency of our PRP reached its steady state value after ∼5 s, which agreed with the rise time estimated by its supplier. In the PRP experiments, we waited for 30 s after changing any parameters to let the recorded hologram reach steady state before taking any measurements.

To evaluate the performances of the system based on either the PRP or BSO crystal as a PCM, we acquired TRUE signals using a 1-cm-thick gelatin-intralipid sample having a reduced scattering coefficient $\mu_s' = 5 \text{ cm}^{-1}$. Figure 2(a) shows the measured peak intensity of the TRUE signal versus the intensity ratio of scattered *S* to *R* in both scenarios. We fixed the *R* and *R** intensities at 10 mW/cm² and 140 mW/cm², respectively, and increased the *S* intensity while monitoring it with PD2. When we changed the PCM, we adjusted mirrors M3 and M4 in Fig. 1(b) to maximize the TR signal at PD1 before taking any measurement. The TRUE signal in this experiment did not show a sharp signal rise accompanied with a fast decay, as in Ref. 2. This is because we used a lower *R** intensity here compared with that in Ref. 2, and the dependence of the TRUE waveform on the *R** intensity was reported previously.[8] It can be seen that the PRP generated signal is ∼8 times stronger than the BSO crystal, thus enabling stronger TRUE focusing.

Seen in Fig. 2(a) is the linear relationship between the TRUE signal and the intensity ratio of scattered *S* to *R*. To understand this linear relationship, we can describe the interferogram as the intensity averaged over the response time of the PRP:

$$I = |r|^2 + |s(x,y)|^2 + 2\,\text{Re}[r^* s_-(x,y)], \quad (1)$$
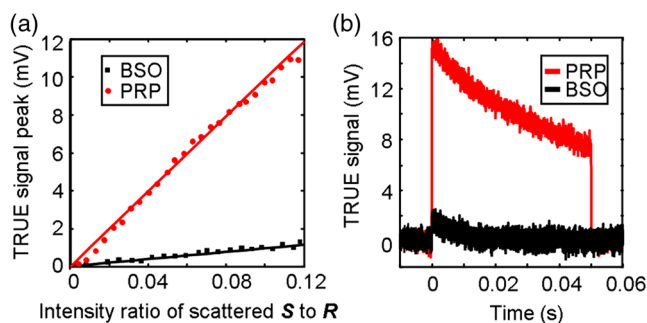

Fig. 2 Comparison of TRUE signals acquired using the PRP and BSO crystal. (a) Plot of measured peak of TRUE signal versus intensity ratio of scattered *S* to *R*. Linear fitting curves are also shown. (b) Representative temporal profiles of TRUE signals acquired using the PRP and BSO crystal.

where *r* and *s* are the complex amplitudes of *R* and scattered *S*, respectively, and s_- is that of down-modulated *S*. Also, r^* denotes the complex conjugate of *r*, and the spatial dependences of *s* and s_- have been explicitly spelled out. Note that interferences between different frequency components are not stationary, and average to zero. The third term in Eq. (1) is the intensity fringe responsible for the hologram recording, and the first two terms are the background. Because $|r|^2$ is much stronger than $|s|^2$, the *s* contribution to the background is negligible. Therefore, the fringe contrast is proportional to the amplitude ratio $|s_-/r|$. From the theory of PR materials, it is known that the holographic diffraction efficiency η is proportional to the squared contrast (or modulation) of the interference fringe that engraves the hologram,[9] i.e., $\eta \propto |s_-/r|^2$. Thus, the TRUE signal linearly increased with $|s_-|^2$ or the *S* intensity while $|r|^2$ was fixed.

Figure 2(b) shows the temporal profiles of TRUE signals generated by PRP and BSO, respectively. In both cases, the power of *S* was 280 mW, and the corresponding intensity ratio of scattered *S* to *R* was 0.14. In addition to the ∼8 times increase in the peak signal intensity, the TRUE signal generated by the PRP lasted ∼10 times longer than that of the BSO crystal as quantified by the time to 50% drop from the maximum. The focused optical energy generated by the PRP was increased by at least 40-fold over the BSO systems reported earlier, as computed by the areas under the curves.

To demonstrate PRP's improved penetration capability, we imaged a phantom sample using TRUE optical focusing. The phantom was a gelatin-intralipid mixture, having a thickness of 1 cm and a reduced scattering coefficient $\mu_s' = 12 \text{ cm}^{-1}$. Embedded in the middle plane of the sample were two optical absorbers Obj1 and Obj2, with thicknesses of 0.5 mm and 0.4 mm along the *Z* axis, respectively, made by adding black India ink to the background solution before it gelled. The absorption coefficients (μ_a) of the turbid background and the optical absorbers were measured to be ∼0.13 cm⁻¹ and ∼8.8 cm⁻¹, respectively. Figure 3(a) shows a photo of the imaging plane containing the two absorbers. The power of *S* was 250 mW, spread over an area of ∼10 mm² on the incident sample surface, whereas the intensity of *R* was 14 mW/cm², and the intensity of *R** was 240 mW/cm². The US transducer was aligned so that its focal zone intersected with the optical axis along *S*. The US beam scanned along *X* across the optical absorbers with a step size of 0.32 mm. The TRUE signal was obtained by subtracting the averaged (32 times) PD1 signal when the US was off from the PD1 signal when the US was on. Figure 3(b) shows the
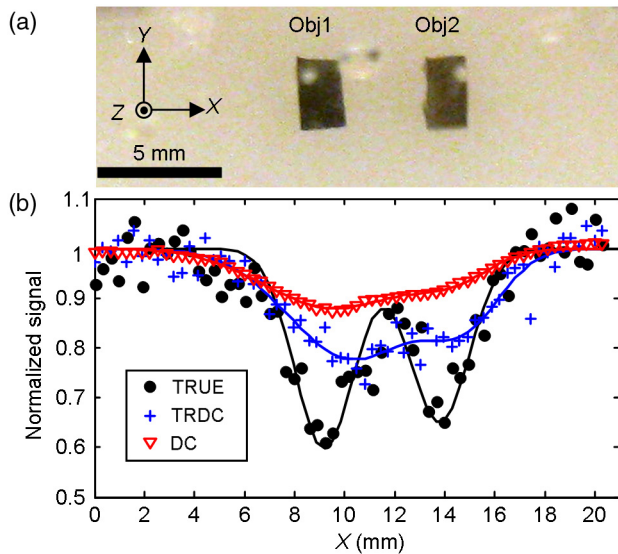
(a)

(b)

Fig. 3 1-D image demonstrating TRUE optical focusing using a PRP. (a) Photograph of the imaging plane. (b) Normalized TRUE signal, TRDC signal, and DC signal versus the X axis.

normalized TRUE signal versus X. As a comparison, we also plotted the normalized distributions of the direct-current (DC) signal, defined as scattered S intensity acquired without US at the PRP position, and the TR direct-current (TRDC) signal acquired as the TR signal without US when S and R share the same frequency. As shown in Fig. 3(b), the TRUE signal drops when the US focal zone intersects the two optical absorbers at $X \sim 9$ mm and 14 mm, respectively. By contrast, the DC and TRDC images do not reveal the two absorbers clearly as a result of the strong light scattering in the sample. The optical thickness of the sample is $(\mu_s + \mu_a) \times d \approx 120$ (d is the geometric thickness of the sample) or $(\mu_s' + \mu_a) \times d \approx 12$, where the anisotropic factor $g \approx 0.9$.[10] The sample thickness presented here far exceeds the maximum penetration previously reported in TRUE imaging experiments,[1,2,11] which illustrates the enhanced energy focused by the PRP.

The PRP used in this study does have drawbacks: signal instability over a long time ($\sim$30 min), a relatively low optical damage threshold ($\sim$250 mW/cm^2), and a slow response time ($\sim$5 s). Also, in certain applications that require rapid scanning of the focal spot, long persistency of the hologram may become undesirable. However, monitoring of the two-wave mixing gain as a reference signal to normalize the measured TRUE signal may compensate for the signal fluctuation. Moreover, maintaining the beam intensity below the PRP damage threshold while expanding the beam size of R and R^* can further increase the focused light intensity. For future *in vivo* experiments, it is necessary to shorten the holographic rise time to within the speckle correlation time of tissue ($\sim$1 ms). Also, to compensate for the slow rise time, we used a continuous-wave US beam in this work, which deteriorates the focal resolution along the acoustic axis (Y axis). In tackling these problems, one may seek to improve the rise time by increasing the R intensity without exceeding the PRP's optical damage threshold. On the other hand, combinations of a pulsed laser and fast PRPs may potentially enable *in vivo* experiments by providing a fast response

and a large active area,[5] while improving the acoustic axial resolution by the use of short synchronized US pulses. It was also reported that applying a higher voltage ($\sim$8 kV) on the polymer accelerates PR response, and thus controls the rise time and persistency to some extent.[4] For tissue penetration, wavelengths in the optical window (approximately 600 to 1300 nm) are more suitable. By choosing the appropriate wavelength sensitive composites, PRPs can be tuned to work within the desired wavelength range.[12] Thus, the disadvantages of the current PRP are likely to be overcome, and its efficient light focusing ability is highly attractive. For example, while the penetration thickness of the one-dimensional (1-D) image presented here was 120, the maximum penetration thickness of a phantom from which we observed a TRUE signal was 200 (data not shown).

In summary, using a PRP considerably enhanced the focused energy in TRUE optical focusing. We demonstrated a 1-D imaging result with TRUE optical focusing at an optical thickness of 120 scattering mean free paths. Further improvement can be expected by increasing the hologram area and using a PRP with faster response time.

References

1. X. Xu, H. Liu, and L. V. Wang, "Time-reversed ultrasonically encoded optical focusing into scattering media," *Nat. Photon.* **5**(3), 154–157 (2011).
2. P. Lai et al., "Reflection-mode time-reversed ultrasonically encoded optical focusing into turbid media," *J. Biomed. Opt.* **16**(8), 080505 (2011).
3. P.-A. Blanche et al., "An updatable holographic display for 3D visualization," *J. Display Technol.* **4**(4), 424–430 (2008).
4. S. Tay et al., "An updatable holographic three-dimensional display," *Nature* **451**(2), 694–698 (2008).
5. M. Eralp et al., "Submillisecond response of a photorefractive polymer under single nanosecond pulse exposure," *Appl. Phys. Lett.* **89**(11), 114105 (2006).
6. S. I. Stepanov and M. P. Petrov, "Efficient unstationary holographic recording in photorefractive crystals under and external alternating electric field," *Opt. Commun.* **53**(5), 292–295 (1985).
7. H. Zhang et al., "Ultrasound-modulated optical tomography using four-wave mixing in photorefractive polymers," *Proc. SPIE* **6856**, 68561S (2008).
8. P. Lai et al., "Time-reversed ultrasonically encoded optical focusing in biological tissue," *J. Biomed. Opt.* **17**(3), 030506, (2012).
9. M. P. Petrov, S. I. Stepanov, and A. V. Khomenko, *Photorefractive Crystals in Coherent Optical Systems*, Springer-Verlag, Berlin, Heidelberg (1991).
10. S. T. Flock et al., "Optical properties of intralipid: a phantom medium for light propagation studies," *Laser. Surg. Med.* **12**(5), 510–519 (1992).
11. H. Liu et al., "Time-reversed ultrasonically encoded optical focusing into tissue-mimicking media with thickness up to 70 mean free paths," *J. Biomed. Opt.* **16**(8), 086009 (2011).
12. M. Eralp et al., "High-performance photorefractive polymer operating at 975 nm," *Appl. Phys. Lett.* **85**(7), 1095–1097 (2004).